THE PREFENTIAL WELD CORROSION OF X65 CARBON STEEL PIPELINE UNDER CO$_2$ ENVIRONMENT

(Korosi Preferensial pada Sambungan Las Pipa Baja Karbon X65 pada Lingkungan Gas Karbondioksida)

Nofrizal[1], Susan .A. Impey,[2] Konstantinos Georgarakis[3]

[1]"LEMIGAS" R & D Centre for Oil and Gas Technology
Jl. Ciledug Raya, Kav. 109, Cipulir, Kebayoran Lama, P.O. Box 1089/JKT, Jakarta Selatan, 12230, Indonesia
Tromol Pos: 6022/KBYB-Jakarta 12120, Telephone: 62-21-7394422, Faxsimile: 62-21-7246150

[2,3] School of Aerospace, Transport and Manufacturing, Cranfield University, Cranfield MK43 0AL. UK

Email: nofrizalsy@gmail.com
First Registered on Februari 7th 2019; Received after Correction on April 11th 2019
Publication Approval on: April 30th2019

ABSTRAK

Korosi Preferensial pada lasan (PWC) adalah bentuk serangan korosi parah yang ditemukan pada sambungan pipa di industri minyak dan gas. PWC terjadi ketika laju korosi logam las (WM) dan zona pengaruh panas (HAZ) lebih tinggi dari logam induk (PM). PWC dihasilkan oleh mekanisme korosi galvanik karena perbedaan dalam komposisi dan mikrostruktur logam di tiga daerah lasan. Tujuan dari penelitian ini adalah untuk mempelajari pengaruh laju aliran pada korosi preferensial lasan (PWC) pada baja pipa kekuatan tinggi X65 menggunakan teknik jet impingement dengan menyelidiki mekanisme PWC pada sambungan lasan pada air laut buatan yang sudah dijenuhkan dengan karbon dioksida pada tekanan 1 bar. Peralatan jet impingement terdiri dari 3 cincin (luar, dalam dan tengah) dirancang sehingga bahan induk, zona yang terkena panas dan logam las dapat dianalisis dalam lingkungan tegangan geser tinggi. Percobaan korosi dilakukan dengan baja pipa X65 dalam kondisi tanpa aliran dan aliran pada 10 m / s pada 30ºC dan pH4. Karakteristik arus galvanik antara daerah-daerah pengelasan dicatat menggunakan resistant ammeter, dan laju korosi dianalisis dengan menggunakan pengukuran resistansi polarisasi linear. Total laju korosi dihitung dari jumlah kontribusi galvanik dan korosi sendiri. Morfologi, struktur, bahan kimia pada permukaan X65 setelah proses korosi diselidiki dengan cara pemindaian mikroskop elektron (SEM) dan focus ion beams (FIB) untuk memeriksa produk korosi yang terbentuk dalam air garam yang mengandung karbon dioksida terlarut. Dalam kondisi tanpa aliran, hasilnya menunjukkan bahwa karakteristik galvanik pada semua lasan sama dan WM bersifat katodik dan dilindungi dibandingkan dengan HAZ dan PM. Dalam kondisi mengalir, taksiran laju aliran terkait dengan berbagai posisi pada target bervariasi tergantung pada (a) PM dan HAZ atau (b) WM. Efek dari laju aliran target pada WM memiliki tren yang sama, tetapi tingkat korosi keseluruhan lebih besar karena PWC. Hasil analisis permukaan setelah proses korosi menunjukkan bahwa penghilangan lapisan yang mengeras dan keretakan di bawah permukaan merupakan penyebab meningkatnya degradasi.

Kata Kunci*: Korosi las preferensial; karbon dioksida; pengukuran elektrokimia; jet impingement*

ABSTRACT

Preferential weld corrosion (PWC) is a severe corrosion form of attack found in pipeline weldments in oil and gas industries. PWC occurs when the corrosion rate of the weld metal (WM) and heat affected zone (HAZ) is higher than the parent metal (PM). PWC was generated by galvanic corrosion mechanism due to dissimilarities in the composition and microstructure of the metal in the three weld regions. The aim of this research is to study the effect of flow rate on preferential weld corrosion (PWC) in X65 high strength pipeline steel using submerged jet impingement by investigating the mechanism of PWC on a weldment in artificial seawater saturated with carbon dioxide at 1 bar. A novel submerged jet impingement apparatus that

consist of 3 rings (outer, inner and centre) was designed so that the parent material, heat affected zone and weld metal could be analysed in a high shear stress environment. Corrosion experiments were performed with X65 pipeline steel under no flow and flowing condition at 10 m/s at 30ºC and pH4. The galvanic current characteristic between the weldment regions was recorded using a zero-resistance ammeter, and the self-corrosion was analysed by using linear polarisation resistance measurements. Total corrosion rates were calculated from the sum of the galvanic and self-corrosion contributions. The morphology, structure, chemical on the surface of X65 after corrosion process was investigated by means of scanning electron microscopy (SEM) and focus ion beam (FIB) to examine the corrosion product that form in brine containing dissolved carbon dioxide. In a no-flow condition, the result shows that the galvanic characteristics on all weldments were similar and the WM is cathodic and protected in comparison with the HAZ and PM. In flowing condition, the estimated flow rates associated with the different positions on the target vary depending on either (a) PM and HAZ or (b) the WM. The effects of target flow rate on WM have a similar trend, but the overall corrosion rates are greater due to PWC. The result of surface analysis after corrosion process showing that removal of hardened layer and subsurface cracking were causes of enhanced degradation.

Keywords: Preferential weld corrosion; carbon dioxide; electrochemical measurements; submerged jet impingement

I. INTRODUCTION

Corrosion is a crucial problem that strongly affects natural and industrial environments around the world. Steel, commonly used to design infrastructures or process facilities in many industries experiences many types of corrosion, and one of the common problems is galvanic corrosion attack.

The study of a specific type of aqueous corrosion behaviour, known as galvanic corrosion of dissimilar metals when coupled together is challenging. Typically, corrosion rates can vary considerably when different materials are combined in static or dynamic aqueous environments. It is more challenging when three or more elements are linked and immersed in a fluid and where flow rates are variable and critical (Lee, et al., 2005 & Mahajanam & Joosten, 2011).

A weldment comprises three different areas, namely parent metal (PM), weld metal (WM) and heat affected zone (HAZ). These areas have small differences in composition and microstructure, but these small differences can be enough to cause preferential weld corrosion (PWC), particularly in a flowing environment. The effect of PWC corrosion in oil and gas, especially in offshore production is particularly detrimental, with the associated marine environment and wide fluctuations in exposure to salt water and temperatures. Figure 1 shows an example of severe PWC in a carbon steel pipeline which failed after only a few months in service (Winning, et al., 2004).

In general, the effects of corrosion attacks on various industries directly affect the economic, technological, safety and environmental sectors around the world. In the UK, the latest study found that the overall financial loss per year due to corrosion of metal reached about 4.5% of the gross national product (GDP) (Bhaskaran, et al., 2005). In the United States, the Federal Highway Administration (FHWA) released a report on corrosion cost in 2000, stating that, in several sectors , the loss incurred as a result of corrosion is approximately $ 257 billion/ year, which is about 3.5% of their GDP (Fontanna, 1986; Ahmad, 2006; Revie & Uhlig, 1985).

In the oil and gas industry, carbon dioxide and hydrogen sulphide can create serious corrosion problems which can destroy process equipment, cause human endangerment, and high financial losses (Lahiri, 2017). Particular attention is required for CO$_2$ corrosion, which can lead to various types of corrosion in oil and gas productions such as localised corrosion in welded materials, these can attack the integrity of the carbon steel pipeline.

It has been reported that the percentage financial loss due to welding failure in the oil pipeline is 60 % of the total corrosion problem (Abduh, 2008; Perez, 2013). In Alaska, during 2006, due to a tiny hole in a pipeline wall, operated by British Petroleum (BP), a result of a corrosion attack, a significant volume of crude oil spilled into the sea. It is estimated that at least a $100 million loss was incurred. The sea's ecosystem was also severely effected as a result of the spill.

In November 2006, a natural gas pipeline in East Java Indonesia with diameter pressure of 440 Psi failed and caused a major explosion. About 11 fatalities were reported and about 25 industrial gas customers were also affected due to this incident (Abduh, 2008). Weld corrosion was identified as responsible for a severe disaster which occurred in 2006 in Prudhoe Bay field North America. A small hole initiated by a weld failure was responsible for 5000 barrels of crude oil contaminating 1.9 acres of sea. British Petroleum incurred losses of up to $320 million including fines for endangering the safety of the environment and the public (Joshua & Yereth, 2009).

It is generally agreed that the location and morphology of weldment attack can be influenced by many parameters, which includes the environment, flow patterns, the composition of the weld metal relative to the parent metal and the welding method, among others (Alawadhi & Robinson, 2011; Adegbite , et al., 2016; Martinez, et al., 2011). However, from the information available and experience, the mechanisms of this corrosion phenomenon are still unclear. The most accepted explanation of selective or preferential corrosion is the difference in composition and microstructure across the weldment. In addition, it is still difficult to predict the weld corrosion rate that may be experienced, the exact location of attack (such as, weld metal and heat affected zone). Care is also needed in applying curative measures for other applications because of the complexity of interacting factors that may lead to additional problems.
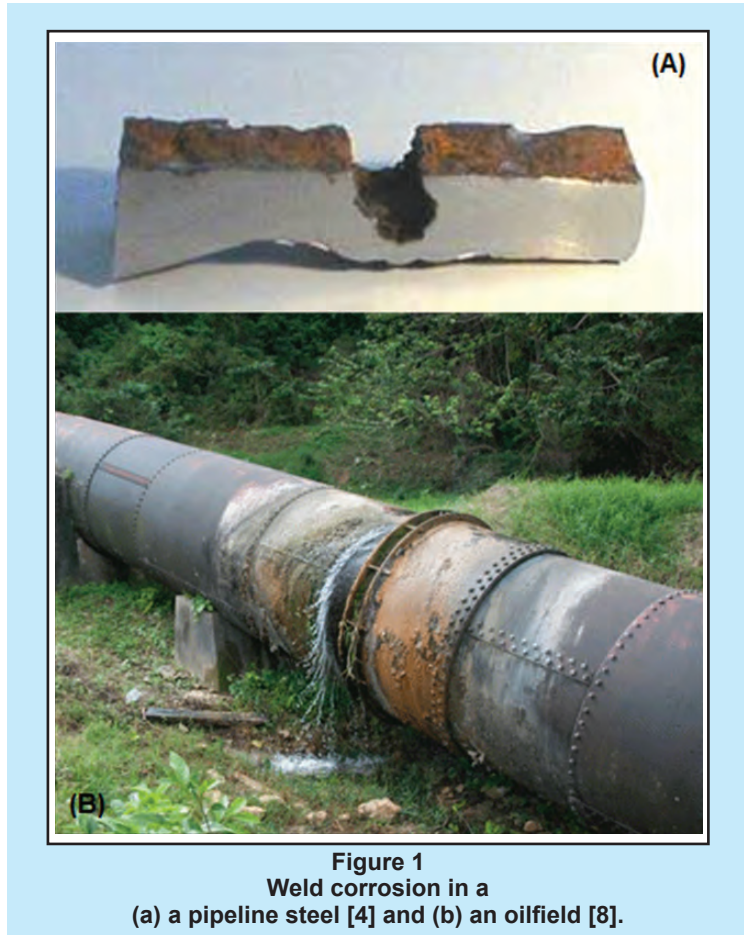

Figure 1
Weld corrosion in a
(a) a pipeline steel [4] and (b) an oilfield [8].

This paper presents an experimental analysis of PWC of carbon steel to develop an understanding of the mechanisms of PWC of X65 carbon steel under CO_2 environment and it contribution to total corrosion degradation. Several surface analysis techniques were used to determine how the properties of carbon steel surfaces were affected by PWC corrosion conditions and how these effects contributed to enhanced rates of degradation. A new weld is studied, having been produced by a different process and using different welding parameters from those employed in previous work (Adegbite, et al., 2016).

II. EXPERIMENTAL

A. Experimental Procedure

1. Materials

A Submerged Jet Impingement (SJI) target was prepared from a sample of X65 pipeline steel with a weldment from a multi-pass welding process. The chemical composition of the parent metal and weld metal is shown in Table 1.

Table 1
Composition of X65 pipeline steel (I) and weld metal (II) (Wt %)

	C	Si	Mn	P	S	N	Al	Cu	Mo	Ni	Cr	Nb	Ti
Pipe (%)	0.07	0.30	1.51	0.01	< 0.005	0.005	0.04	0.26	0.01	0.39	0.02	0.02	< 0.01
Weld (%)	0.07	0.30	1.59	0.01	0.007	0.005	< 0.01	0.1	0.11	0.27	0.03	< 0.01	< 0.01

The weldment plate (Figure 2A-B), of area 210 x 60 mm^2 and 30 mm thickness, was polished using different grades of abrasive paper from 240 to 1200 grit, rinsed with deionized water, isopropanol then etched in 10 % Nital. The detailed macrostructure of X65 weldment is shown in Figure 2C showing parent metal (PM), weld metal (WM) and heat affected zone (HAZ).

2. Design and Construction of the Submerged Jet Impingement (SJI) Target

The SJI target design used in this study is adopted from previous work by Adegbite et al., (2016) and shown in Figure 3A. The target for this current research is constructed from carefully selected sections, extracted with electrical discharge machining (EDM) from the X65 carbon steel pipeline weldment of three weld metal (WM), three heat affected zone (HAZ) and three parent material sections (PM) with surface areas in the ratio 2:1:8 respectively (Figure 3B).

Each of the nine metal pieces were attached to a connector and then later an electrical wire to create an electrode. The target was formed of three concentric circles, each with a section of parent metal, weld metal and heat affected zone, isolated from neighbouring sections with PTFE to avoid electrical contact (shown in Figure 4A and 4B). The concentric circles are placed so as to experience different hydrodynamic effects from an impinging water jet. The target form was filled with insulating resin. Wires connected to the electrodes were combined and protected in an insulated cable as shown in Figure 4C.
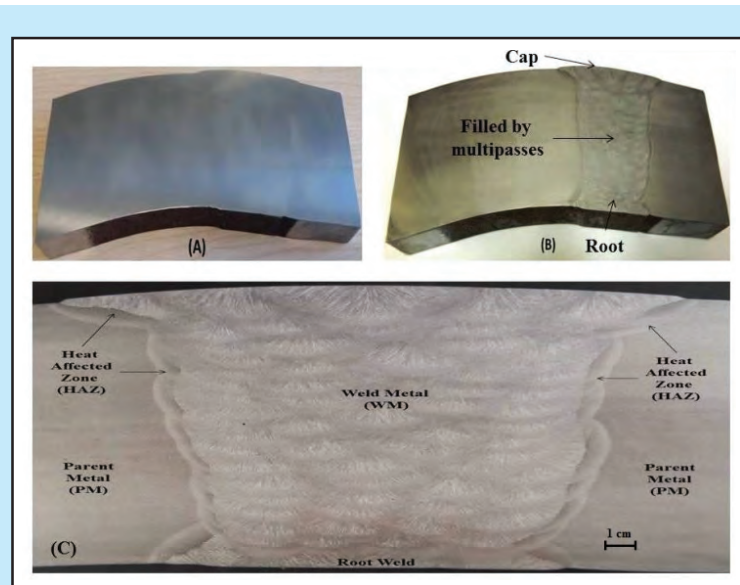

Figure 2
(A) Welded plate, (B) plate etched in 10 % Nital and (C) PM, WM and HAZ macrostructure.

B. Experiment Procedure

The SJI target was polished using different grades of abrasive paper from 240 up to 1200, rinsed with deionized water and isopropanol then dried. All tests were performed in both static conditions and with a flow rate of 10 m/s in artificial seawater saturated with CO_2.

The experimental layout of submerged jet impingement used in this research is shown schematically in Figure 5. The SJI target is placed in a glass cell within a flow loop, beneath a 5 mm water jet nozzle. The cell also contains reference and auxiliary electrodes and is connected to a zero resistance ammeter to monitor the corrosion process.

Initially, brine solution is deaerated with N_2 in a glass cell for 4 hours to remove the dissolved oxygen in the system. Then CO_2 is sparged into the flow loop for 12 hours for effective saturation. After 12 hours brine solution saturated with CO_2 flowing at 10 m/s is applied with the jet

onto the submerged target. The flow loop temperature is maintained at $30^{\circ}C$ while CO_2 is bubbled into the system continuously for the experiment duration.

C. Electrochemical Measurements

Galvanic currents: The galvanic currents between each weld region were recorded every minute using a multi-channel zero resistance ammeter (ZRA), ACM Instrument Galvo-Gill 12) connected to a data logging PC. For the nine electrode sections in each hydrodynamic region of the target, currents from the parent material (PM) to the heat-affected zone (HAZ) and from the weld metal (WM) to the HAZ were recorded on six channels of the ZRA. The working electrodes were coupled, with the HAZ short-circuiting all channels. The reference electrode (SCE) was connected to all channels in the same way as the HAZ. Since the three working electrodes (PM, HAZ, WM) were in the short circuit condition, the sum of their individual galvanic currents will be zero, such that their individual galvanic currents (I_{PM}, I_{HAZ}, I_{WM} respectively) are established from the following relationship:

$$I_{PM} + I_{HAZ} + I_{WM} = 0 \qquad (1)$$

D. Self-Corrosion Rates:

Self-corrosion rates of the Submerged Jet Impingent (SJI) target were analysed from linear polarisation resistance measurements of each working electrode. The LPR was determined by using every single section in the SJI target as a working electrode with a standard calomel reference electrode (SCE) and an auxillary platinum electrode. A cyclic sweep technique is used to scan each uncoupled electrode from 10 mV (SCE) below the open circuit potential (OCP) to 10 mV (SCE) above the OCP and back to the starting potential.
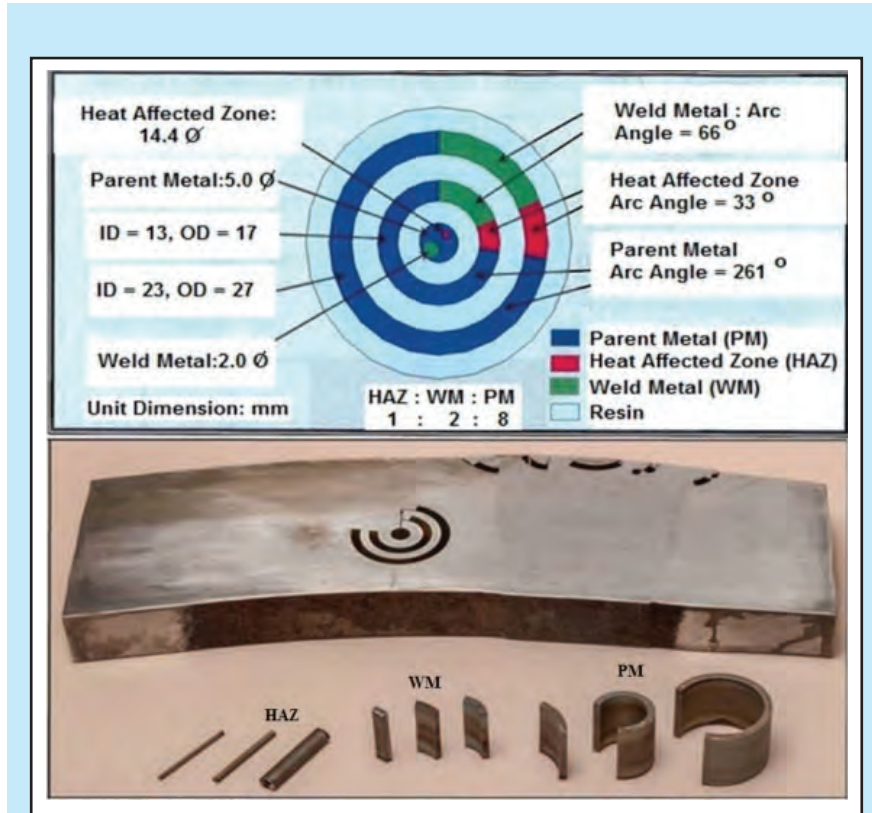

Figure 3
(A) Design of jet impingement target [14]; (B) the sections of weldment cut using electrical discharge machining (EDM).

Changes of current during the process were recorded every second.

The resulting potential/current density plot exhibited a straight line where the gradient is inversely related to the corrosion rate. This results in the polarisation resistance Rp, which is related to the corrosion current using Equation 2:

$$Rp = \Delta E / \Delta I = ß/(Icorr) \qquad (2)$$

Where:

Rp $\quad$ = polarisation resistance (Ωcm^2)

Icorr $\quad$ = corrosion current (A/cm^2)

ß $\quad$ = Stern-Geary constant related to the anodic (b_a) and cathodic (b_c) Tafel slopes. ß value is 26 (Domingguez, et al., 2016; Gaurav, 2015; Owen, et al., 2018).

E. Electrochemical Impedance Spectroscopy (EIS)

Electrochemical impedance spectroscopy was used to complement the LPR measurements and

confirm the self-corrosion rates. The potential was scanned +/- 10mV of the open circuit potential, as in the LPR measurements, at frequencies ranging from 20kHz to 0.05 Hz and the corresponding currents were recorded and used to calculate the impedance of the corrosion processes. In addition, EIS can be used to investigate the corrosion mechanism and the influence of surface films that result from either the corrosion process or the action of the inhibitor.

F. Scanning Electron Microscopy (SEM-EDX)

SEM is a qualitative surface analysis technique used to observe surfaces of carbon steel samples exposed to a brine solution saturated with CO_2 in a range of conditions for 20 hours. Samples for SEM analysis were prepared from parts of the X65 carbon steel weldment.

Before analysis, the corroded sample was rinsed and cleaned with isopropanol and deionised water, dried and stored in a desiccator prior to the SEM analysis. Analysis was performed using a Philips-XL30 SEM with energy dispersive x-ray analysis (EDX) The data obtained was analysed with Aztec software from Oxford Instruments.
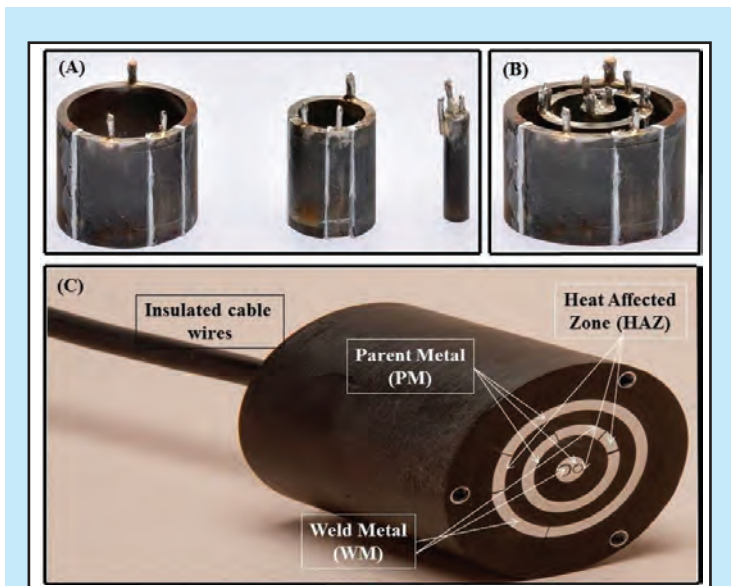

Figure 4
(A) Three concentric rings each with three electrode sections electrically isolated (B) positioning the ring sections for the target and (C) completed SJI target electrically connected and filled with resin.
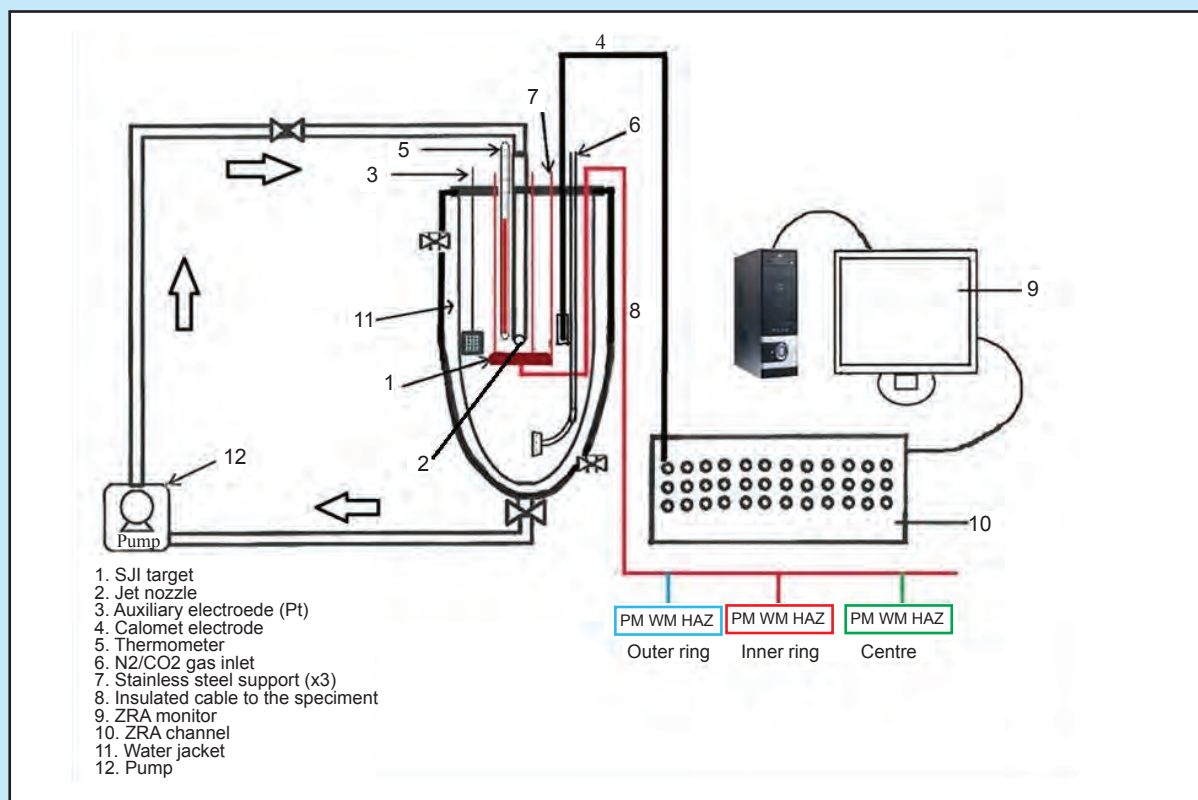

1. SJI target
2. Jet nozzle
3. Auxiliary electroede (Pt)
4. Calomet electrode
5. Thermometer
6. N2/CO2 gas inlet
7. Stainless steel support (x3)
8. Insulated cable to the speciment
9. ZRA monitor
10. ZRA channel
11. Water jacket
12. Pump

Figure 5
Schematic of submerged jet impingement layout.

III. RESULTS AND DISCUSSION

Typical results are reported here for the corrosion measurements on the outer ring of the SJI target at a flow rate of 10 m/s using brine solution that saturated with CO_2 without addition of inhibitor (uninhibited environment) and a temperature of 30^oC.

A. Galvanic Current Measurements

The results of the galvanic current measurements are given in Figure 7. During the initial deaeration stage with nitrogen (A), the galvanic currents density are small and slowly decrease. The deaeration is monitored by recording the electrode potentials, which become more electronegative as dissolved oxygen is removed. Figure 6 shows that the potentials of the PM/HAZ couples are lowered to approximately-550 mV(SCE) during this period. The brine solution is considered to be well deaerated when the potential reaches -740 mV(SCE) and thus, in these initial experiments, there is no dissolved oxygen present (Alawadhi & Robinson, 2011; Adegbite, et al., 2016; Martinez, et al., 2011).

When CO_2 is bubbled into the cell (B), there is a further active shift in the electrode potentials to -754 mV(SCE) as the steel electrodes are attacked by the carbonic acid (Figure 6) accompanied by changing in the galvanic currents density (Figure 7). At this stage, the PM is slightly anodic to the other two weld regions (a positive current) and the WM and HAZ are both cathodic (negative currents) and therefore partially protected from corrosion.

After flowing CO_2 into the solution for 6h, the pump is started and the brine impinges on the target electrodes at 10 m/s (C). There is a large transient increase in the galvanic currents, which quickly stabilises, leaving a reversal in the current direction on the WM. Whereas the WM has been cathodic in static conditions,
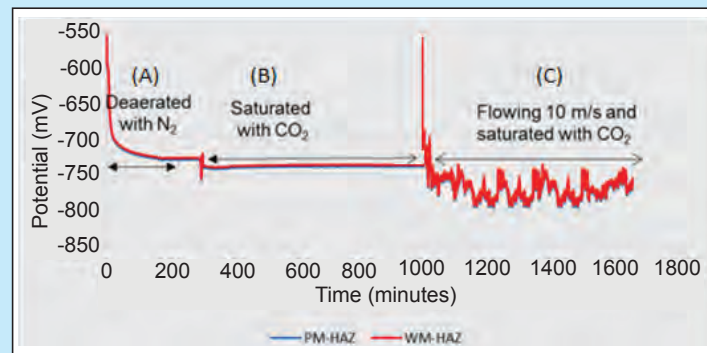

Figure 6
Corrosion potential of PM-HAZ galvanic couples in stagnant brine solution (b) saturated with CO_2 and (c) flowing at 10 m/s and 30 ^{o}C.
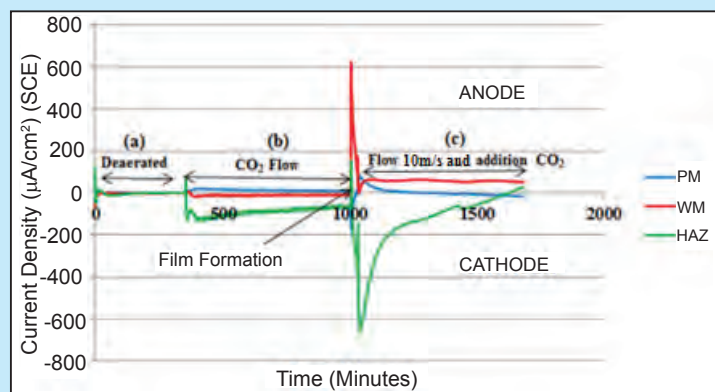

Figure 7
Galvanic current density in the weld sections exposed to (a)static deaerated brine solution, then (b) saturated with CO_2, and (c) flowing at 10 m/s and 30 ^{o}C.
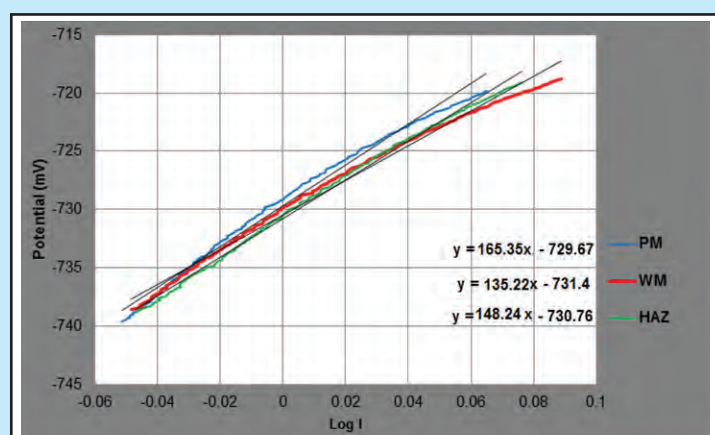

Figure 8
The plot of cyclic sweep measurements for weld sections of the outer ring in brine saturated with CO_2 at10 m/s flow rate and 30 ^{o}C.

it now becomes anodic, providing corrosion protection mainly to the HAZ. If sustained over long periods,

this current reversal would result in the preferential corrosion of the WM.

The galvanic current density was observed at the end of the period from values of corrosion current density of WM, HAZ and PM are 60, 45, and -25 $\mu A/cm^2$, respectively. The characteristics of galvanic (coupled) interactions between the PM, WM, and the HAZ when coupled occurring in this experiment have similar trends to previously reported studies on X65. Research by Lee, et al., (2005) found that the WM (0.7 % nickel) is protected by the galvanic current of PM and WM in a still condition. However, in a flowing condition at 1000 rpm the WM became anodic corroding preferentially.

Tests conducted by Barker et al. and (Owen, et al., 2018) found that over 5 hours of immersion in a no-flow condition, the PM remained in anodic whereas WM containing 1% nickel was cathodic. However, the situation changed once in a flowing environment where the WM and HAZ became anodic and vulnerable to preferential corrosion. Alawadhi and Robinson, (2011) also obtained similar results. Their experiment ran for three days in sweet corrosion (CO_2) conditions using an RCE at 1000 rpm. Their results showed the WM (0.7 % nickel) is anodic for two days but, on day 3 the position shifted and the HAZ had a slightly positive current compared to the WM. Research by Turgoose et al. (2005), was conducted with a similar SJI target with 0.7-1 % nickel in the weld. The same results are achieved in a flowing condition where the WM and HAZ corroded and protected the PM from corrosion attack.

B. Self-Corrosion Measurements

Linear polarisation resistance (LPR) measurements for all of the electrodes are recorded after the galvanic measurements were completed and
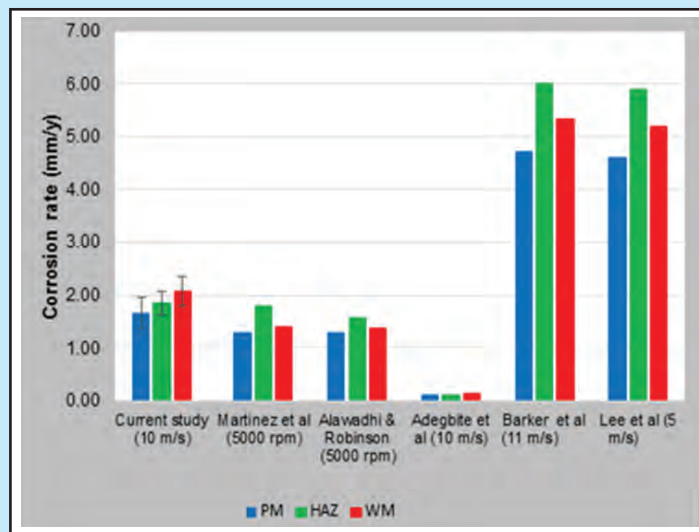

Figure 9
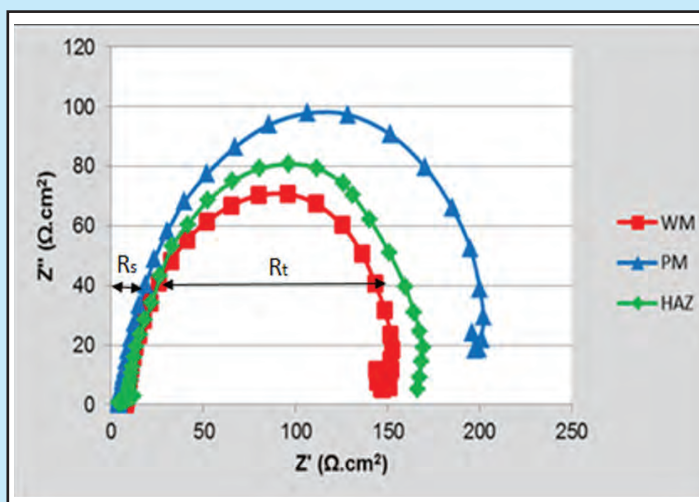**Self-corrosion rates from the current study on X65 weldment and comparison with literature.**

Figure 10
Nyquist plots of weld sections of the outer ring in brine saturated with CO_2 at 10 m/s flow rate and 30 °C.

Table 2
LPR characteristics for the outer ring of the target in uninhibited brine with CO_2 at 10 m/s (taken from Figure 8)

	Weld section	E_{corr} (mV)	i_{corr} ($\mu A/cm^2$)	Corrosion rate (mm/y)
Outer	PM	-729	157.3	1.9
	HAZ	-730	175.9	2
	WM	-730	192	2.2

typical potential/current density plots for the outer ring are shown in Figure 8. The open circuit potentials of the

electrodes (where current density is zero) confirm that the WM was the most electronegative of the three weld regions and therefore it behaves as the anode in the galvanic current measurements.

For each electrode, the polarisation resistance was calculated from the gradient of the potential/current density plot and used to obtain the corrosion current density and the self-corrosion rate using Equation 2.

Table 2 shows the self-corrosion rate for the outer ring of the target in uninhibited brine with CO_2 at 10 m/s (taken from Figure 8).

At flowing 10 m/s, the WM is active with the lowest LPR value or highest corrosion current density. I_{corr} for the PM, the HAZ and the WM with a 10 m/s jet are 157, 175 and 192 $\mu A/cm^2$ respectively, compared with 91-95 $\mu A/cm2$ under static (no flow) conditions (the figure is not showed). Thus, a flowing environment increases the corrosion current density.

From Table 2 shows the self-corrosion rate of the PM and HAZ were close to each other (1.9 -2.0 mm/y). This value is understandable as they have the same chemical composition but differ in microstructure. The WM has the highest self-corrosion rate at about 2.2 mm/y. This means the WM has lower corrosion resistance compared to the PM and HAZ under the studied flowing conditions.

The tendency of WM or HAZ to be more anodic in turbulent uninhibited brine occurs in all previous studies even with different welds or steel compositions. Based on the compositions for this study given in Table 1, the WM has a slightly lower Ni content (0.24 wt%) compared to the PM (0.36 wt%).

In Figure 9, self-corrosion rates of an X65 steel weldment from a flowing condition are compared to previous research reported in the literature. The comparison is complex due to variations weld composition, flow and local environment with the differing techniques. In a flowing condition, the shear stress plays a significant role on the rate of corrosion rate of the weldment.

Although in most studies weldments of different composition are used, three studies report using the same X65 weldment. Martinez et al. (2011) uses a rotating cylinder electrode at 5000 rpm (70 Pa shear stress) and reports results for PM, HAZ, and WM of 1.3; 1.8 and 1.4 mm/year. Alawadhi & Robinson (2011), using the same method as Martinez, at 5000 rpm (70 Pa shear stress), found similar corrosion rate results for WM and PM of 1.3 and 1.4 mm/y, while the HAZ has a high corrosion rate at 1.6 mm/y (compared with Martinez) despite the lower flow rate.

Barker, et al., (2013) found that the corrosion rate of PM, WM and HAZ in uninhibited brine saturated with CO2 with the electrolyte flowing at 11 m/s was 4.7; 5.3 and 6.02 mm/y respectively. Another study from Lee, et al., 2005 using at velocity 5 m/s resulted in corrosion rates for the PM, HAZ and WM in a range 4.2-6.2 mm/y. For both of these studies, while the trend is equivalent, the results are high compared to other reported studies. Likely explanation for the high rates could be from the position of the weldment compared to the jet or more likely, the presence of a very small amount of dissolved oxygen in the system which will accelerate a corrosion reaction at the anodic side (Alawadhi & Robinson, 2011; Adegbite, et al., 2016; Martinez, et al., 2011)

A significant difference was found in Adegbite's et al. (2016) research. He uses a similar flow rate to this current study (10 m/s or 280 Pa of shear stress). Corrosion rates for the PM, the HAZ and the WM are in a range 0.13-0.19 mm/y (Figure 10). This result is significantly different from work of others using the same material (X65).

Table 3

Impedance measurement for outer ring at 10 m/s

Flow	Weldment area	R_s	R_t	R_s+R_t	LPR value	Corrosion Rate EIS (mm/y)	Corrosion Rate LPR (mm/y)
10 (m/s)	PM	4.8±0.77	173.2±2.8	178.4	165.4	1.70±0.14	1.82±0.21
	HAZ	5.8±0.56	150.5±2.4	156.3	148.7	1.91±0.13	2.06±0.11
	WM	6.9±0.81	131.7±2.6	138.5	132.4	2.12±0.22	2.22±0.25

The results from all studies gathered above, show that attacks on the HAZ or WM are a common occurrence in weldments in uninhibited flowing brine saturated with CO_2. Attack on the WM or the HAZ occurs in flowing conditions in every study even though each weldment was manufactured from an X65 carbon steel with a different chemical composition or different microstructure.

C. Electrochemical Impedance Spectroscopy (EIS)

Nyquist plots for the three weld regions in the outer electrode ring are shown in Figure 10. Essentially, each consists of a single, complete semicircle indicating that corrosion occurred by an activation controlled process. There was no evidence of a second semicircle at high frequencies, which would suggest the presence of a corrosion product film on the metal surface.

The diameter of the semicircle represents the charge transfer resistance, R_t, while, the R_s is represent as an electrolyte resistance (the value of R_s+R_t is broadly equivalent to the polarization resistance measured in the LPR technique) from which the corrosion current density and self-corrosion rate can be obtained using Equation 2. The resistance values obtained by the two methods show good agreement (Table 3).

The WM had the lowest charge transfer resistance (R_t) of around 131 $\Omega.cm^2$ at 10 m/s. The highest rate of self-corrosion is experienced by the WM (2.2 mm/y) compared to the PM (1.8 mm/y) and HAZ (2.0 mm/y). The R_s+R_t values for the PM and the HAZ at 178 and 156 $\Omega.cm^2$ respectively, were found.

D. Total Corrosion Rate

The total corrosion rate for each section of the weldment is calculated from the sum of coupled (galvanic) corrosion and uncoupled (self) corrosion measurements.

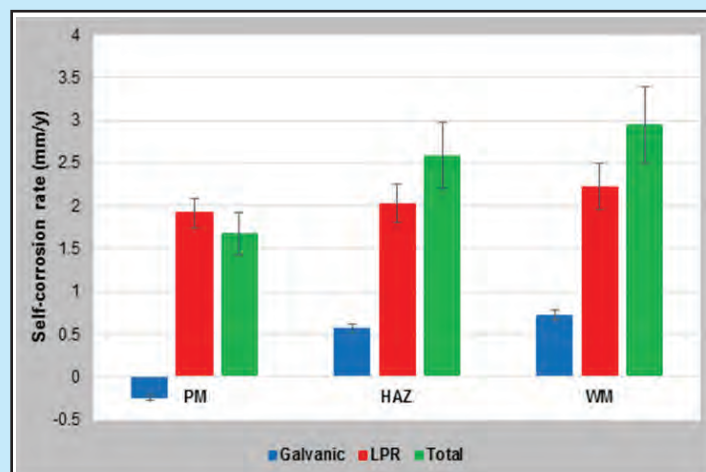$$CR\ Total\ =\ CR_{Galv}+CR_{Self} \qquad (3)$$

Figure 11
Total corrosion rate in weld sections of the outer ring in brine saturated with CO_2 at 10 m/s flow rate and 30°C.
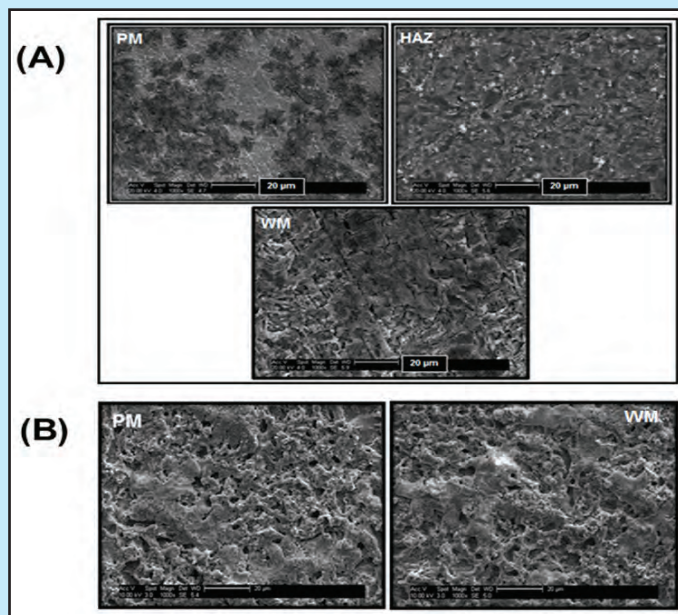

Figure 12
Typical SEM micrographs of the weldment after exposure to brine saturated with CO_2 (a) at 10 m/s (b) with no flow.

The overall corrosion rates for each electrode in the outer ring in a flowing brine environment saturated with CO_2 at 10 m/s is shown in Figure 11.

The total corrosion rates (in green) of the WM in each electrode in the outer ring exceeded that of the PM and HAZ. In contrast, the PM and HAZ will corrode less than the WM, in some cases at 30-23% of the rate of the WM. Thus in an environment of uninhibited brine saturated with the CO_2 at 10 m/s, preferential weld corrosion (PWC) is expected to occur.

Figure 11 shows galvanic protection of the PM results in a slight reduction of the total corrosion rate. Thus in the outer electrodes, the PM is noble, with a lower total corrosion rate, compared to the WM and the HAZ. The self-corrosion rates of the WM, the HAZ and the PM differ, with values in the outer rings in the range 1.9, 2.0 and 2.2 mm/y for the PM, the HAZ and the WM, respectively. There was a significant increase in self-corrosion compared to stagnant conditions as described in the previous chapter. However, the difference in self-corrosion between the three electrodes is not too high because he three electrodes are located in the same hydrodynamic region.

The total corrosion rate of PM and HAZ in the outer region is in the range 1.7-2.5 mm/y. The WM has highest total corrosion rate at 2.8 mm/y, and the weld is vulnerable to corrosion in the oil and gas process from preferential or localized corrosion in the weld area.

E. Surface Characterisation

To monitor the change of morphology and to investigate the details of chemical composition of the weld and/or a carbonate or oxide that could form

Table 4
EDX analysis of the weldment in the outer ring in uninhibited brine

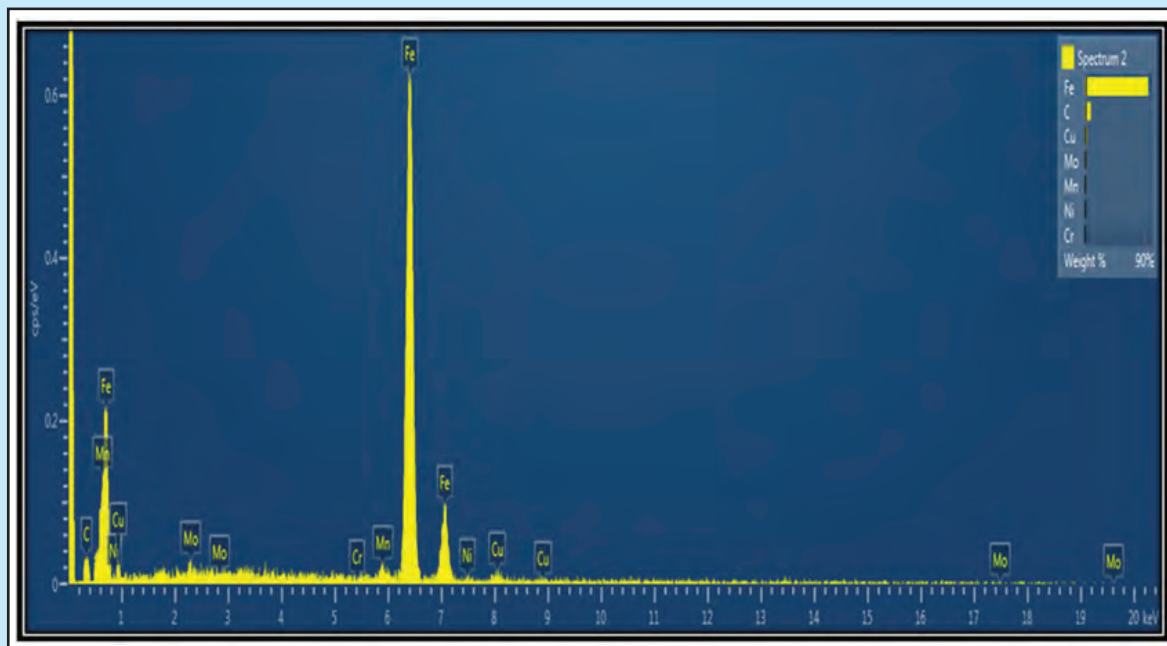| Elements	PM (wt %)		WM (wt %)	
	Not corroded (fresh metal)	Corroded with flow	Not corroded (fresh metal)	Corroded with flow
C	0.7	15.4	0.9	19.8
Si	0.1	0.2	0.3	0.2
Mn	1.6	1.4	1.7	1.6
Ni	0.3	0.4	0.2	0.3
Cu	0.2	0.3	0.2	0.2
Fe	97.1	82.3	96.7	77.9
Total	100	100	100	100

Figure 13
The EDX chromatograms for PM in uninhibited brine flowing 10 m/s saturated with CO_2 environment.
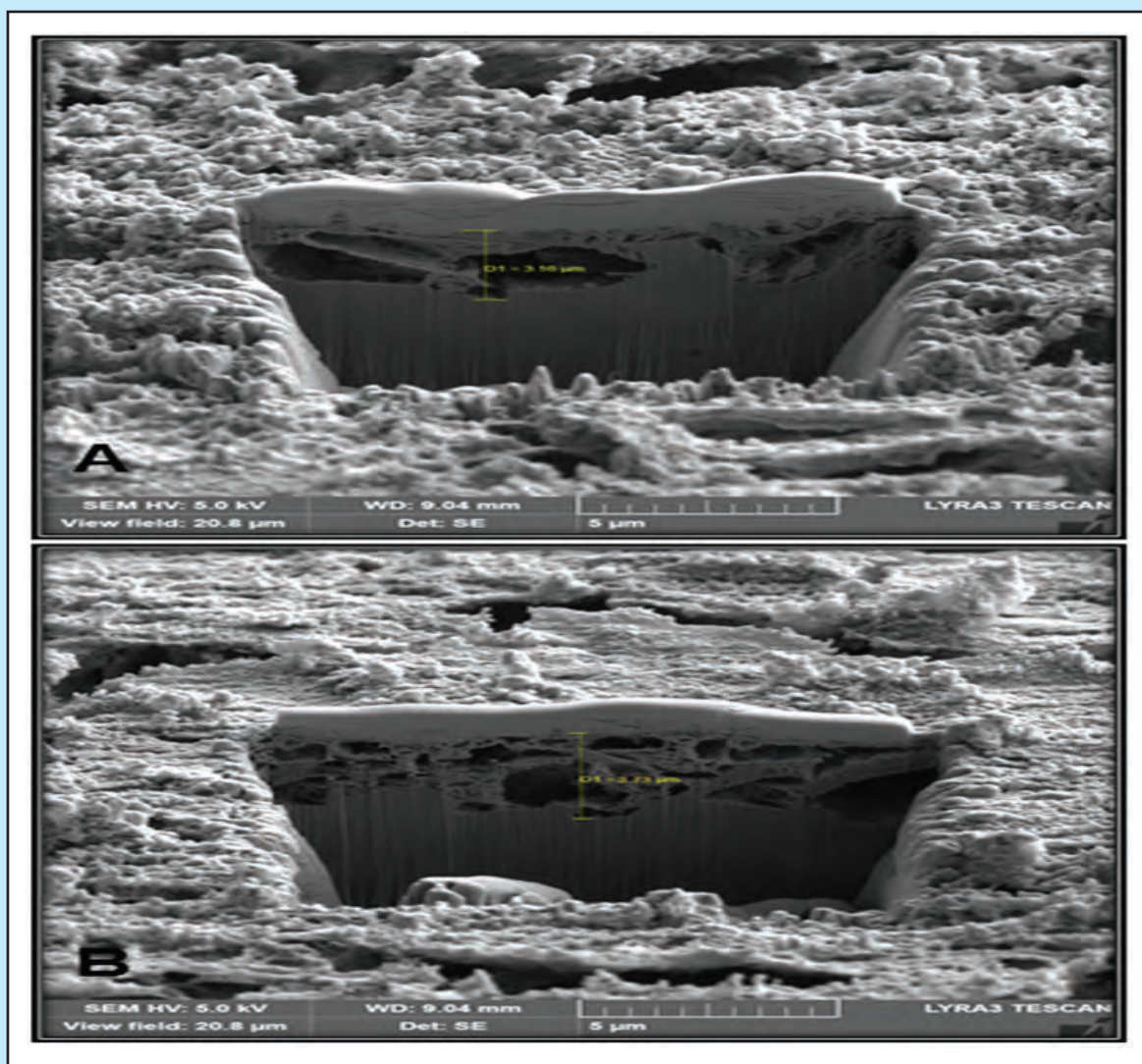
Figure 14
The FIB micrograph of the parent metal (A)
and the weld metal (B) in uninhibited flowing 10 m/s saturated with CO_2.

on the surface of the weld and to understand the mechanism of corrosion, SEM and elemental analysis using energy dispersive spectrometry (EDX) is employed.

For surface analysis purposes, a weldment sample was exposed to SJI with uninhibited brine solution saturated with CO_2 for 20 hours under a flowing brine solution at 10 m/s. After that, the weldment was washed with deionised water, rinsed using isopropanol and dried. The surface was then analysed with Scanning Electron Microscopy (Philips-XL30 ESEM with EDX). The aim was to assess the morphology and composition of the corroded surface (corrosion product) as if it was the SJI target.

Figure 12 shows SEM micrographs of the PM, the WM and the HAZ. In the flowing environment, the surface of the WM and the HAZ appear rough and damaged, less on the PM. Pits and cracks have formed in the HAZ and WM. In the flowing conditions, due to high shear stress, areas of the weldment were unprotected resulting in greater material loss than no-flow conditions. Material dissolution with the removal of ferrite leaves cementite regions at the surface. The result is similar to that of Hu et al. (2011) using X-65 at flow rate 7 m/s. They note material dissolution is the dominant process rather than material removal through particle impingement (Burkle, et al., 2017).

The surface elemental composition from EDX spectra (Figure 13) are given in Table 4, with the

elemental composition of the PM, the WM and the HAZ after corrosion. The accumulation of carbon on the corroded ample is significant compared to fresh material. The carbon concentration on the weldment was 15.4 and 19.6 wt % for the PM and the WM respectively.

The concentration of Fe in the weldment decreases with the corrosion reaction and more Fe dissolves in the brine solution. In this case iron (Fe) depletes from 97 and 96 wt% for the PM and the WM in fresh sample to 82 and 77 for PM and WM after corrosion process. The decrease in Fe concentration in flowing conditions is accompanied by a rise in carbon. There is no indication of oxygen presence on the steel. This supports the argument that the corrosion mechanism is primarily related with the dissolution of Fe without the formation of oxygen containing film or corrosion products on the corroded surface.

The elemental compositions in Table 4 support those from electrochemical measurements showing the WM has a higher corrosion rate with more Fe dissolving into the corrosive media. In this condition formation of protective film on the weldment surface such as $FeCO_3$ is not favoured.

SEM studies in the literature on coupled weldments exposed in flowing conditions also reported the absence of a protective film $FeCO_3$ despite higher temperatures to this study (Fontana, 1986; Abduh, 2008). The study of Alawadhi & Robinson (2011) was performed at flowing condition of RCE at 5000 rpm, and 40 °C. The SJI study by Adegbite et al. (2016) was at 30-40°C.

Focus Ion Beam (FIB) sections are taken to observe the effect of fluid turbulence on the SJI target, reproduced on weldment surfaces. Figure 14 shows a FIB section of the weld metal (WM). A porous and significantly depleted zone at the near surface is observed beneath a protective Pt layer. This depleted zone is about 3.8 μm thick for the WM (Figure 14A) and 2.5-3 μm thick for the PM (Figure 14B). This support the accelerated corrosion attack measured using the electrochemical method particularly with self-corrosion measurements.

Barker et al. 2012, found that the PM was nobler than the HAZ and the WM. They noted that the effect of microstructure and the composition play a significant role during the corrosion process. Similar results were found by Alawadhi and Robinson 2011, who used the RCE method at 5000 rpm. They found a lower corrosion rate on the PM compared to HAZ and WM in flowing conditions. However they argued that a $FeCO_3$ film and cementite phase could reinforce the protective film and anchor it to the PM.

V. CONCLUSIONS

From these experiments, it can be summarised that:

In artificial sea-water saturated with CO_2 at flowing conditions of 10 m/s, the weld metal becomes anodic and preferentially corrodes in comparison to the parent metal. The PM and HAZ will corrode less than the WM, in some cases at 30-23% of the rate of the WM. Thus in an environment of uninhibited brine saturated with the CO_2 at 10 m/s, preferential weld corrosion (PWC) is expected to occur.

Galvanic corrosion plays a significant contribution to the total corrosion in a flowing environment where the WM and the HAZ are anodic. As the current density is calculated from the current divided with each electrode area, a tiny area of HAZ and WM will produce a high current density. Therefore, they corroded faster compared to the PM and result in Preferential Weld Corrosion (PWC).

SEM and FIB results show that the dissolution of ferrite leaves porous cementite (Fe_3C) at the surface particularly in a flowing uninhibited environment. No evidence of a $FeCO_3$ film was found in this study.

The presence of even small quantities of dissolved oxygen in brine containing carbon dioxide can increase the overall rate of corrosion of steel and this can result in serious damage in pipework systems from leaks at pumps and valves.

ACKNOWLEDGEMENTS

REFERENCES

Abduh, M., 2008. The 50 major engineering failures in oil and gas and hydrocarbon industry (1977-2007). [Online] Available at: https://www.scribd.com/document/215642171/The-50-Major-Engineering-Failures [Accessed 2008].

Adegbite , M. A., Robinson, M. J. & **Impey, S. A**., 2016. Evaluation of Flow Enhanced Preferential Weld Corrosion of X65 Pipeline Steel Using a Novel

Submerged Impingement Jet. Society of Petroleum Engineers, 2-4 August.

Ahmad, Z., 2006. Principles of Corrosion Engineering and Corrosion Control. 1st ed. s.l.:Butterworth-Heinemann, Elsevier.

Alawadhi, K. & **Robinson, M. J.**, 2011. Preferential weld corrosion of X65 pipeline steel in flowing brines containing carbon dioxide. The International Journal of Corrosion Processes and Corrosion Control, 46(4), pp. 318-329.

Barker, R., Hu, . X., Neville, A. & **Cushnaghan, S**., 2013. Assessment of Preferential Weld Corrosion of Carbon Steel Pipework in CO2-Saturated Flow-Induced Corrosion Environments. Corrosion The Journal of Science and Engineering, November, 69(11), pp. 1132-1143.

Bhaskaran, R., Palaniswamy, N., Rengaswamy, . N. & **Jayachandran, M**., 2005. A review of differing approaches used to estimate the cost of corrosion (and their relevance in the development of modern corrosion prevention and control strategies). Anti-Corrosion Methods and Materials, 52(1), pp. 29-41.

Burkle, D. et al., 2017. In situ SR-XRD study of $FeCO_3$ precipitation kinetics onto carbon steel in CO_2-containing environments: The influence of brine pH. Electrochimica Acta, November, Volume 255, pp. 127-144.

Domínguez Olivo, J., Brown, B. & **Nesic, S**., 2016. Modeling of Corrosion Mechanisms in the Presence of Quaternary. Houston, Texas, NACE Internation, Publication Division.

Fontana, M. G., 1986. Corrosion Engineering. 3rd ed. Boston, MA: McGraw-Hill Book Company.

Hu, X., Barker, R., Neville, A. & **Gnanavelu, A.**, 2011. Case study on erosion–corrosion degradation of pipework located on an offshore oil and gas facility. Wear, 29 July, 271(9-10), pp. 1295-1301.

Joosten, M. W., **Kolts, Juri**, **Kiefer, Joseph**, **Humble, Philip G.**, & **Marlow, John A.**, 1996. Aspects of Selective Weld and HAZ Attack in CO_2 Containing Production Environments. Corrosion, 24-29 March.

Joshi, G. R., 2015. Elucidating Sweet Corrosion Scales. Manchester, UK: The University of Manchester.

J**oshua Schneyer** & **Yereth Rosen**, 2009. Reuters. [Online] Available at: https://www.reuters.com/article/bp-alaska-spill/update-4-oil-leak-has-minimal-impact-on-bps-alaska-output-idUSN3045041520091201

Lahiri, A. K., 2017. Applied Metallurgy and Corrosion Control. s.l.:Springer, Singapore.

Lee, C., Bond, S. & **Woollin, P**., 2005. Preferential weld corosion: Effects of weldment microstructure and composition. CORROSION.

Mahajanam, S. P. & **Joosten, M. W.**, 2011. Guidelines for Filler-Material Selection To Minimize Preferential Weld Corrosion in Pipeline Steels. SPE Projects, Facilities & Construction, March.6(01).

Martinez, M. et al., 2011. Control of Preferential Weld Corrosion of X65 Pipeline Steel In Flowing Brines Containing Carbon Dioxide. CORROSION, 13-17 March.

Owen, J., Ramsey, C., Barker, R. & **Neville, A**., 2018. Erosion-corrosion interactions of X65 carbon steel in aqueous CO2 environments. WEAR, November, Volume 414-415, pp. 376-389.

Revie, R. W. & **Uhlig, H. H**., 1985. Corrosion and Corrosion Control. Ottawa: WILEY & Sons, Inc..

Turgoose, S. & **Palmer , J. W.**, 2005. Preferential Weld Corrosion of 1% Ni Welds: Effects of Solution Conductivity and Corrosion Inhibitors. Houston, Texas, NACE International.

Winning, I. G., Mcnaughtan, D. & **Bretherton, N.**, 2004. Evaluation of Weld Corrosion Behavior and the Application of Corrosion Inhibitors and Combined Scale/Corrosion Inhibitors. CORROSION, 28 March-1 April.